LARGER-SCALE STRUCTURE IN THE TURBULENT BOUNDARY LAYER

Nick Hutchins, Kwing-So Choi
School of Mechanical, Materials, Manufacturing Engineering and Management
University of Nottingham, University Park, Nottingham, NG7 2RD, UK
E-mail address: Kwing-So.Choi@Nottingham.ac.uk

ABSTRACT

An experimental study using hot-wire based measurement and novel conditional analysis techniques has revealed interesting large-scale features in the turbulent boundary layer. It is found that a hierarchy of hairpin-type events characterise the logarithmic and wake regions. To the best of the authors' knowledge, such structures have not previously been experimentally measured in their entirety. At all detection heights, we find that these resolved structures maintain a presence in the viscous sublayer (i.e they have a distinctive near-wall footprint). Statistically we find a decay in the detection frequency with increasing distance from the wall. Also interesting, is tentative evidence for the existence of a preferred spacing mode for these events. Regardless of detection height, this spacing remains approximately constant at $x^+ \approx 300$. This is a surprising result, and seems to tally with the near-wall spacing implied by the time between successive VITA detected events (for near-wall quasi-streamwise structures). These results are preliminary and we would urgently seek to test the existence of these spacing modes in higher *Re* flows. However, for the time being, the implication seems to be that a spacing, which was originally prescribed in the near-wall region, is maintained as the near-wall structure grows / mutates into the hairpin hierarchy that we find to predominate all the way from the buffer region to the edge of the turbulent boundary layer (δ).

INTRODUCTION

The work described here attempts to add to existing knowledge of coherent structures in the canonical turbulent boundary layer. The current study was undertaken within the Drag Reduction Group at the University of Nottingham, under the broad long-term goal of producing novel skin friction reduction strategies. In terms of flow control, we would ultimately aim to learn more about the roles played by these structures in turbulence production and the generation of wall-shear stress. To this end, the coherent structure is also analysed in a TBL that has been manipulated to give skin friction reduction (using a device that is not altogether dissimilar to a LEBU - see Hutchins and Choi 2002). However, for the present report we will concentrate exclusively on the canonical case.

Countless other studies have set out to investigate the coherent structure. Extensive (although not exhaustive) reviews of this work can be found in Robinson (1991) and Panton (2001a, 2001b). However, it is fair to say that until fairly recently, the vast majority of this work has tended to concentrate on those structures in the near-wall region. Near-wall structures have an obvious attraction for several reasons. At the low Reynolds numbers typical of many laboratory investigations they are the single most obvious contributors to turbulence production, accounting for the large peak occurring near the wall. From the point of view of manipulation, many turbulent control techniques are wall-based, and hence the near-wall structure seems an obvious target. Further to this, the clearest available view of the temporally developing coherent structure invariably comes courtesy of DNS results. By definition such results are of very low Reynolds number flows, typically channel flows with a half-height of the order 150 wall units. In these instances the logarithmic region of the flow is practically non-existent, and there is very little separation between the smallest and largest scales (often making the larger-scale structures far from obvious in these studies). In spite of such limitations, the images provided by DNS experiments have proven remarkably persuasive. As researchers, there is a danger that we will be seduced by the wealth of low Reynolds number data, with the result that the near-wall predominantly streamwise coherent structure becomes the sole focus of our attention (the 'lure of the wall' perhaps?). However, we must not become blind to the wider picture. For example it is an often cited fact that 50% of the turbulence production occurs in the first few percent of the boundary layer (the buffer layer). This is certainly true at the low Reynolds numbers discussed by Kline *et al.* (1967). However, this fact alone does not necessarily mean that we should ignore the remaining 50%. Indeed, as Reynolds number increases, so the dominance of the near-wall region will be diminished. At some point the integrated production occurring across the logarithmic region will exceed that in the buffer region (see Adrian 2002). In addition to this, recent results, indicating that larger-scale structures can occasionally be arranged in well organised groups, have suggested that these logarithmic scales might be much more significant in terms of Reynolds stresses, transport and production mechanisms than previously anticipated (Christensen and Adrian 2001; Adrian *et al.* 2000; Marušić 2001). As such it seems likely that these larger scale structures could have an important role to play in future turbulence control strategies.

EXPERIMENTAL SET-UP

Experiments are performed in an open return low speed wind tunnel with a 300 mm × 534 mm working section of total length 4.5 m. The boundary layer was tripped near the inlet of the working section ensuring a fully-developed turbulent boundary layer over the test surface. The test surface is an unbroken Perspex plate of 12 mm overall thickness and length 2.0 m mounted approximately 2.5 m downstream of the inlet. The freestream velocity is 2.5 m s^{-1} , with a turbulence intensity of approximately 0.3%. The Reynolds numbers at the test section measurement stations range from

$1080 \lesssim Re_\theta \lesssim 1500$ ($420 \lesssim Re_\tau \lesssim 550$). All velocity measurements are made using constant temperature hot-wire anemometry. The traversing probe measures the streamwise velocity component using a miniature boundary layer type hot-wire probe (55P15) controlled by a Dantec 56C CTA. The static (detection) probe is a 55P61 uv x-wire sensor controlled by a pair of Dantec 54T30 mini CTAs, providing streamwise and wall-normal velocity components. All probes have 1.25 mm-long sensing elements of 5 μm-diameter and hot-wires are operated in constant-temperature mode with the overheat ratio set to 1.8. Data from the anemometer system were sampled at a rate of 1 kHz using an IOTech ADC 488/8S analogue-to-digital converter. The traversing probe is mounted to a three-axis traverse mechanism, which is computer controlled via a Digiplan step-motor controller. Wall normal (y-axis) movements are made with a resolution of 1.25 μm. Figure 3 shows a schematic of the probe array used to detect the large scale structure.

DETECTION SCHEME

An alternative trigger is required to extract the coherent vortical structure from the logarithmic and wake regions of the turbulent boundary layer. Many of the existing detection techniques become unpredictable in this region. VITA tends to detect on strong inclined shear-layers (high $\partial u/\partial t$), U-level on strong accelerations or decelerations (large positive or negative u), whilst threshold quadrant techniques detect on ejection or sweep-type events. All of these techniques have proven rather effective at extracting the near-wall quasi-streamwise structure (due mainly to the large shear in this region). However, away from the wall, none of these have a detection signature that is uniquely associated with the presence (or passage) of larger-scale lifted structures. To analyse structural features in this region it has proven necessary to develop novel and more reliable detection techniques. The key to this has been a detection scheme based on the spanwise vortices that were so evident in Adrian *et al.*'s (2000) PIV frames, and which they judged to be the heads of lifted hairpin vortex structures. A hot-wire detection scheme to target these events has been developed. Initial development and validation was performed using Adrian *et al.*'s (2000) PIV database, whereby pseudo hot-wire detection schemes could be tested and perfected computationally, (using the existing data), prior to resorting to the wind tunnel. In this way a good deal of laborious experimental development work has been avoided. It should be noted that the use of pre-existing PIV data is an ideal environment in which to develop HWA detection schemes. Given sufficient patience, it should theoretically be possible to design a hot-wire array and detection algorithm to extract any visually observed recurrent features noted in a set of PIV frames. For our purposes we wanted the detection scheme to be as simple as possible (minimum number of sensor elements).

In their PIV frames, Adrian *et al.* (2000) found isolated islands of strong negative ω_z (often, but not always, approximately circular in profile). When the correct convection velocity is subtracted from the uv vectors, approximately *circular streamline* patterns can be revealed around these vorticity concentrations. This is the essence of the vortex identifier employed by Adrian *et al.* (instantaneous negative ω_z concentrations coupled with the existence of circulation or swirl). Realising such a scheme using hot-wire anemometry would be complicated. Instantaneous vorticity is a notoriously difficult measurement to make (as is the confirmation of instantaneous swirl). Instead we seek simpler methods to extract these features.

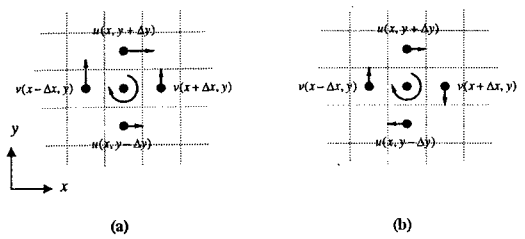

Figure 1: (a) example of spanwise vorticity; (b) spanwise vortex with circular streamlines.

Figure 1(a) and (b) highlight the important difference between spanwise *vorticity* and a spanwise *vortex*. These simple flows have the background shear subtracted (to leave only the fluctuating component). Note that whilst Figure 1(a) shows a negative ω_z, the streamlines can never be circular regardless of the convection velocity used. Hence by the above definition, plot (a) would not constitute a spanwise vortex. The notion of circular streamlines about the central point, implies that the wall-normal velocities upstream and downstream of the detection point will be approximately equal but opposite in magnitude (as in plot b). Thus as a starting point we set out to look at just this scenario, analysing situations in the PIV data where the wall-normal velocity signal (at a given detection height y_1) fluctuates from $-Ku_\tau$ to $+Ku_\tau$ over a suitably short length-scale X (where K and X are the detection variables, threshold and window length respectively). After some initial experimentation, whereby single point detections are visually corroborated against the wider PIV flow field to ensure successful targeting of spanwise vortices, it is found that K and X^+ should be O(1) and O(50) respectively.

In the end result the scheme is promising. Figure 2 shows the resultant ensemble averages at the five different heights when the detection scheme is applied to the PIV data. A spanwise vortex has been resolved at all five y_1 positions. The number of detections from all available frames ranges from 35 at $y_1^+ \approx 110$ to only 6 at $y_1^+ \approx 450$, hence with insufficient realisations the ensemble average can become messy at larger y^+. Regardless, the scheme achieves the

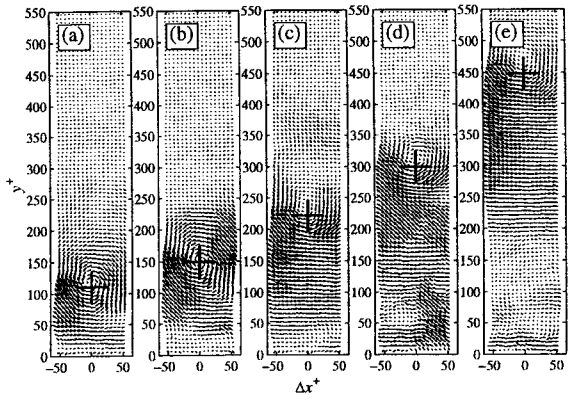

Figure 2: Ensemble averaged signatures from v component detection at (a) $y^+ \approx 110$; (b) $y^+ \approx 150$; (c) $y^+ \approx 225$; (d) $y^+ \approx 300$; (e) $y^+ \approx 450$. Detection simulated in Adrian *et al.*'s PIV database.

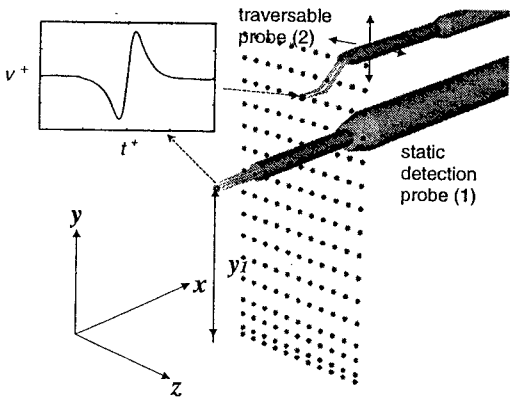

Figure 3: Hot-wire probe array for measurement of intermediate structure.

stated objective, extracting spanwise vortical motions from the PIV frames. Adrian *et al.* (2000) interpreted these spanwise vortices and their spatial distribution to be indicative of the heads of lifted hairpin vortices arranged in packets. The evidence they present for this is rigorous, yet ultimately somewhat limited by being based solely on 2-D observations. Armed with the developed detection scheme we hoped to be able to test the hairpin scenario and by conditionally sampling to either side (in the z direction) of a detected spanwise vortex, expand the model into three dimensions.

For experimental hot-wire application of this scheme we employ Taylor's hypothesis, approximating the spanwise vorticity in terms of the temporally developing wall-normal component at the fixed detection point,

$$\omega_z = \frac{1}{2}\left[\frac{\partial v}{\partial x} - \frac{\partial u}{\partial y}\right] = \frac{1}{2}\left[-\frac{1}{c_x}\frac{\partial v}{\partial t} - \frac{\partial u}{\partial y}\right] \qquad (1)$$

Figure 3 shows the probe array used for subsequent experiments. A uv x-wire sensor (1) is positioned at the detection height y_1 to detect the passage of spanwise vortices at this location. A further traversing single-wire sensor is used to map the fluctuating u component over the datagrid as shown. At each measurement station both probes (three sensor elements in total) are sampled simultaneously at 1kHz for 600 s. This equates to a sample interval of $\Delta t^+ \approx 0.8$ and a sample length of $s_o = (s.U_\infty/\delta_{99}) = 2.5 \times 10^4$. Although in reality the conditional analysis is conducted during post-processing, the basic premise of the detection scheme can be represented on Figure 3. Probe (2) is conditionally sampled upon detection of a fluctuating wall-normal component v^+ at probe (1) switching from $-K$ to $+K$ within a suitably short timescale (established for experiment at $2.5 \lesssim T^+ \lesssim 3.5$, where T is the temporal detection window). In this way probe (1) detects the passage of a spanwise vortex, whilst probe (2) is used to construct an image of any wider associated coherence. Redundant symmetries are avoided by only sampling on the positive z side of the detection plane[1]. After initial trials, a full program of 5 individual experiments was conducted, comprising event detection at $y^+ \approx 110, 150, 220, 300, 450$ ($y = 15, 20, 30, 40, 60$ mm) for the canonical turbulent boundary layers (this was later repeated for the manipulated case).

[1]Even so, each asymmetric data plane takes upwards of 48 hours to acquire, producing up to 2GB of binary signal per experiment.

RESOLVED VORTICAL STRUCTURE

We will concentrate initially on the canonical case detections made at $y_1^+ = 220$, in order that some of the finer points of the scheme can be highlighted.

After conditional sampling, we are left with the ensemble averaged fluctuating u velocity component in z, y and t coordinates (where $t = 0$ is the detection point). Without the provision of further planes in x, the streamwise dimension must be recovered from the temporal development through the measurement plane. Taylor's hypothesis is applied (using a convection velocity based on the local mean at the detection height) to transpose the data into a spatial frame. Applying Taylor's Hypothesis in this way involves the inherent assumption that the coherent structure is a static event (an event that exhibits no temporal evolution other than a constant advection in the streamwise direction). In reality, it has previously been established (see Robinson 1991; Panton 2001a, 2001b) that coherent structures can exhibit stretching, growth, spanwise meandering, local intensifying and dissipation. Hence at larger timeshift values, the accuracy of the transformation must be considered diminished. In effect, we make the tentative assumption that any structural evolution occurs over a greater timescale than the ensemble period. As a first approximation, this seems reasonable when dealing with larger-scale structures.

Once the three-dimensional spatial view of the event has been reconstructed, isosurfaces are drawn through regions of locally accelerated and decelerated flow. These are shown by the dark and light shaded regions in Figure 4. Note from the contour levels that these events are relatively weak in terms of ensemble averaged streamwise velocity fluctuations, which are of the order of a few percent of the local mean. To some extent this weakness was always expected. Even at the detection point (or just above and below if we consider the circular streamlines of Figure 1), the streamwise fluctuation would be expected to be approximately equal to the v trigger, giving $\langle u \rangle = \pm K$. This equates to a percentage streamwise fluctuation of approximately 6% at detection. Obviously as probe (2) is moved further from probe (1) we would expect the correlation between signals to diminish, and this clearly occurs. Nonetheless, within these weak

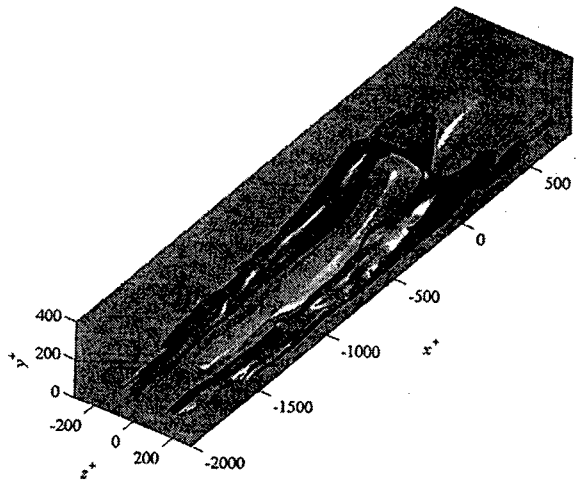

Figure 4: Isosurface plots of smoothed ensemble averaged u fluctuation associated with spanwise vortex detection at $y_1^+ \approx 220$. Isocontours show ■ $(\langle u \rangle / u) = 0.45\%$ (local accelerations); ▒ $(\langle u \rangle / u) = -0.6\%$ (local decelerations).

fluctuations, a predominant and distinct wider structure is clearly observed.

The resolved pattern of increased and reduced velocity is entirely consistent with the velocity fluctuations induced by a lifted hairpin vortex in a shear layer. Figure 5 shows an idealised view of such a structure. At the detection point, the head of the hairpin forms a brief section of spanwise vortex creating a region of increased streamwise velocity above the core, and reductions below. A similar scenario exists on the neck or shoulders of the hairpin. In this region, on the outboard side of the structure a component of the induced velocity acts to increase the local mean $\langle u \rangle$. In contrast, within the loop of the vortex neck, the induced velocity acts against the mean to locally reduce $\langle u \rangle$. The trailing legs are unique in that they lie much closer to the wall, and hence are in a region of high shear. The common-flow-up and common-flow-down sides of these predominantly streamwise vortices will produce regions of reduced and increased velocity respectively (due to Q2 and Q4 pumping). In this way the entire region within the loop of the hairpin ought to be characterised by reduced velocity. Similarly the outside boundary of the structure should be bordered by a region of increased velocity. This is exactly the pattern we see from Figure 4.

In theory, we would expect the vortical structure to exist somewhere between the regions of reduced and increased velocity, specifically at the point of maximum shear. Without v or w data (remember, only $\langle u \rangle$ was measured by probe 2) it is not possible to calculate the three ensemble averaged vorticity components (which could show the vortex location). However, for spanwise and wall-normal vorticity components, the streamwise fluctuation is a suitable tracer, and we can say as an approximation that (in terms of sign),

$$\omega_y \propto \frac{\partial u}{\partial z}, \qquad \omega_z \propto -\frac{\partial u}{\partial y} \tag{2}$$

In other words, when $\partial u/\partial y$ is large positive, there is a strong possibility of a negative signed spanwise vortex. Similarly, where $\partial u/\partial z$ is large positive, we might expect positive wall-normal vortical activity. Streamwise vorticity does not classically involve a u gradient. Salvation comes from the fact that these streamwise vortices would be expected to predominate near the wall. In this region the occurrence of high shear will lead to Q2 and Q4 type interactions (on the respective common-flow-up and down sides of the vortices). For near-wall coherent motion, negative v will be accompanied by positive u, and *vice verse*. Hence we can approximate,

$$\frac{\partial v}{\partial z} \propto -\frac{\partial u}{\partial z}, \qquad \therefore \qquad \omega_x \propto \frac{\partial u}{\partial z} \tag{3}$$

Thus, near the wall, a large positive signed $\partial u/\partial z$ is indicative of a positive signed streamwise vortex.

The 'legs' and 'neck' of the vortex structure will be likely to reside in regions where the absolute value of ω_x and ω_y are large (either large positive, for the positive z half of the domain, or large negative for the negative z half of the domain). Across the entire domain the head of the structure will be located where ω_z is large negative. Thus using the relationships derived in Eq. 2 and 3, the vortical marker function (Ψ_{hp}) is proposed.

$$\Psi_{hp} = \sqrt{\underbrace{\left(\frac{\partial\left(\frac{\langle u \rangle}{u}\right)}{\partial z}\right)^2}_{\pm(\omega_x \ \& \ \omega_y)} + \underbrace{\left(\frac{\partial\left(\frac{\langle u \rangle}{u}\right)}{\partial y}\right)^2}_{-\omega_z}}_{+ve} \tag{4}$$

Eq. 4 can be considered as a very approximate vortical marker for hairpin structures (or if we prefer a measure of internal shear within the ensemble averaged domain). The function Ψ_{hp} is calculated at every grid point over the domain. At locations where large values of Ψ_{hp} are encountered, a hairpin structure is likely to be present. Figure 6 shows an isosurface drawn through the resulting volume at a suitably high level, revealing a clear underlying hairpin form. Obviously Ψ_{hp} represents a compromise. Certainly we have made far-reaching assumptions in arriving at Eq. 4. However, in the absence of full three-component measurements, Figure 6 would seem to indicate that the scheme is successful at extracting the approximate vortical form responsible for the ensemble averaged streamwise velocity fluctuations.

Unlike DNS, flow visualisations or PIV, hot-wire measurements make possible the acquisition of very long signal lengths. This enables a conditionally averaged (and statistically stable) view of the coherent structure to be resolved. Not only do we use the outlined detection scheme to confirm the existence of hairpin structures (later we will present evidence to show that the hairpin template permeates throughout the turbulent boundary layer), but we are

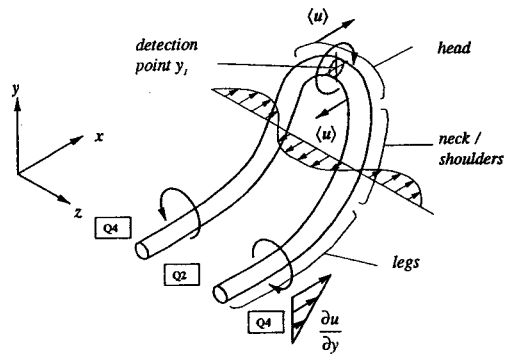

Figure 5: Velocity fluctuation and nomenclature associated with a lifted hairpin vortex.

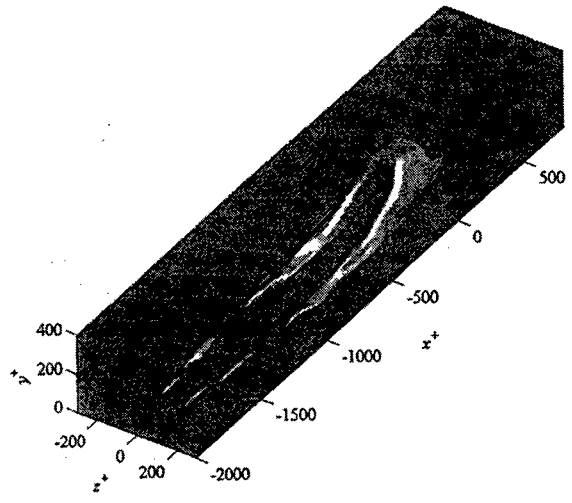

Figure 6: Isosurface showing the dominant vortical structure as detected at $y_1^+ \approx 220$ using the vortical marker function with $\langle \Psi_{hp} \rangle = 150$.

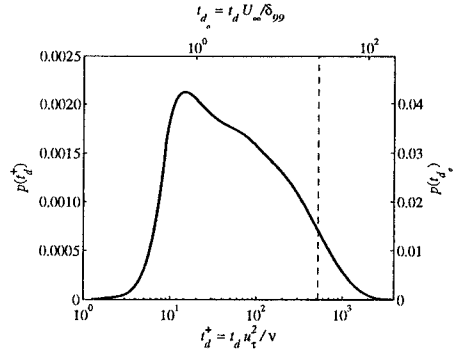

Figure 7: The normalised probability distribution for time between successive hairpin detections t_d plotted on logarithmic time axes.

also able to make more detailed observations of the size, magnitude and population of these events. Of particular interest is the analysis of the time between successive hairpin detections, which we are going to define as t_d. Over the course of the 255 sampling stations (each sampled for 10 minutes), more than 240,000 detections were made (at $y_1^+ \approx 220$). Thus, we have a substantial dataset available. Figure 7 shows the normalised probability for the detected range of t_d. The time has been scaled with both viscous and external scaling (t_d^+ and t_{d_o} respectively). The mean t_d is represented by the dashed line, revealing immediately that the distribution is highly skewed. Clearly, to discuss these events merely in terms of mean detection frequency is somewhat misleading. The distinct modal peak occurring close to $t_d^+ \approx 15$, seems to suggest that these events can commonly occur in 'trains' or 'groups'. At this height ($y_1^+ \approx 220$) the event is assumed to be convecting at close to $c_v^+ \approx 19$, which for the modal peak implies a 'preferred separation' distance of 285 wall units. It should be noted that any notion of 'preferred separation' is quite distinct from Adrian *et al.*'s (2000) packet scenario. In this case we are specifically discussing the streamwise separation between successive hairpin structures with heads located at the same given distance from the wall. However, numerous instances of such separations are evident in the PIV frames of Adrian *et al.*(2000). In particular we refer to their Figures 9, 11, 15, 16 & 17 as all exhibiting instances where pairs of spanwise vortices at a given height from the wall are separated by a comparable streamwise distance. A literature review of previous work can reveal other incidences where spacings of $x^+ \approx 300$ appear to prevail. Bogard and Tiederman (1986) found similar modal behaviour in their study of near-wall ejections, whilst Schoppa and Hussain (2000) produced a conceptual model that involved a clear $x^+ \approx 300$ lengthscale. In their streak-

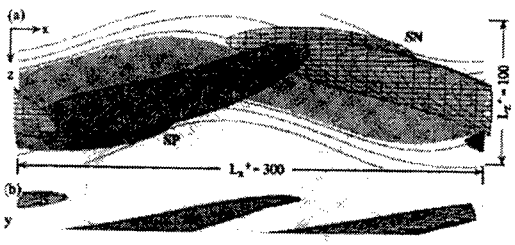

Figure 8: Streamwise vortices generated from the destabilised streak of Schoppa and Hussain (2000).

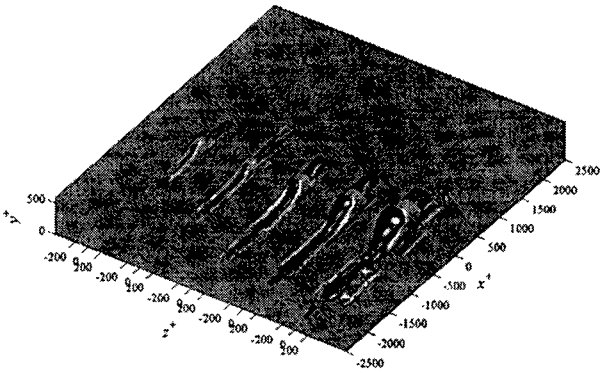

Figure 9: A view of ▒ the resolved vortical structure ($\langle \Psi_{hp} \rangle = 150$) and ■ accompanying low speed region ($\langle u \rangle / u = -0.45\%$) across the range of detection heights (Detection height increasing from $y_1^+ \approx 110$ far-left to $y_1^+ \approx 450$ far-right).

cycle model they showed a near-wall procession of staggered and inclined quasi-streamwise vortices, of alternating sign and located about a common low-speed streak (see Figure 8). As this structure evolves, the downstream tips of the vortices begin to tilt into the spanwise direction to form spanwise vortices (cane-type structures). The sign of rotation determines tilt such that ω_z is always negative (the same as mean shear). This means that in Figure 8, the darker shaded vortex with positive sign (SP) will produce a 'head' at the downstream tip, growing in the negative z direction. Since this is an alternating (repeated) structure, the dimensions given by Schoppa and Hussain (2000) would seem to indicate a separation distance between successive spanwise vortices of approximately $x^+ \approx 300$ on the positive and negative flanks of the low speed streak.

THE RESOLVED STRUCTURE AT ALL DETECTION STATIONS

The detection scheme was applied at five detection stations throughout the log and wake regions of the canonical turbulent boundary layer ($y_1^+ \approx 110$, 150, 220, 300 & 450). Figure 9 shows the resolved structure across this range (the dark and light isosurfaces show the decelerated region, and the approximate vortical form given by Ψ_{hp} respectively). A similar hairpin template is resolved at all detection stations, with the width of the structures seeming to increase in proportion to the detection height. At the largest scale, the

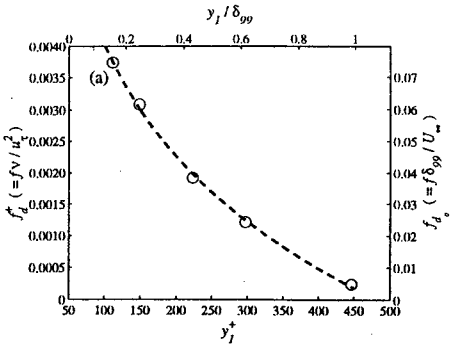

Figure 10: (Variation in event detection frequency ($f = (\overline{t_d})^{-1}$) with detection height.

structure appears to be somewhat 'out of shape'. However, this is probably just a statistical anomaly due to a reduced set of detections in this location. Indeed, Figure 10 clearly indicates a substantial reduction in the detection frequency (hairpin population) as the scale of the structure increases (such that at $y_1^+ \approx 450$ the hairpin detection frequency is only 6% of that found at $y_1^+ \approx 110$). Similar modal tendencies to those shown in Figure 7 are noted across the entire detection range (the modal t_d^+ multiplied by the local convection velocity c_v^+ suggests consistent streamwise spacings of $x^+ \approx 300$).

Further analysis of Figure 9 reveals some additional trends. In general, the smaller hairpin structures tend to be located towards the upstream end of the low-speed region, whilst the larger-scales tend to be shifted more towards the downstream end. In addition, for the smaller scales there is evidence of some streamwise vortical activity *upstream* of the hairpin head (in addition to the trailing legs). Together, this might be taken as circumstantial evidence for the packet scenario as presented by Adrian *et al.* (2000). Finally, although the result is not shown here, it should be noted that all of the detected structures, from $y_1^+ \approx 110$ right the way out to the edge of the boundary layer, maintain a weakly resolved 'footprint' in the extreme near-wall region. These measurements were made at $y^+ \approx 4$, and although the fluctuations are weak, the resolved pattern is clear. In general this footprint is comprised of a low speed region formed beneath the head of the structure (under the spanwise vortex section), and also in the common-flow-up region between the trailing quasi-streamwise legs. Outboard of the legs we see regions of increased velocity due to common-flow-down or Q4 pumping. This shows that even the very largest hairpin structures, that have lifted to the edge of the boundary layer, can maintain a presence in (and impose fluctuations on) the viscous sublayer.

DISCUSSION

It is revealed that the spanwise vortices, so clearly evident in the PIV frames of Adrian *et al.* (2000), are indeed the heads of lifted hairpin structures. Moreover, we find evidence of hairpin structures at all wall-normal locations tested, from the inner log-region to the very edge of boundary layer (and later beyond). These are prevalent features in the turbulent boundary layer, with detection frequencies indicating a dense population of such structures. In fact a very simple statistical analysis indicates that the density of hairpin structures saturates the boundary layer to such a degree that some form of overlapping or 'nesting' is likely to occur. This is seen as supportive of Adrian *et al.*'s (2000) packet scenario (although at this stage the evidence is circumstantial). A clear structural hierarchy exists, with the width of hairpin structures increasing as they are lifted further from the wall. The population seems to diminish with y (although care must be exercised since the detection parameters, threshold K and window size T, can effect detection frequency).

A surprising facet of the resolved hairpin structure is that, at all scales, they retain an influence in the viscous sublayer. This is true even for the largest (and presumably, *oldest*) scales that have grown to the very edge of the boundary layer. The over-riding impression is of lifted attached eddies; a hairpin structure that has grown to the edge of the boundary layer, yet is still dragging its feet (or to be precise, trailing its legs) through the near-wall region to cause low and high-speed streaks. In this way, it is seen that even the largest structures are imposing disturbances on the near-wall region.

Equally surprising is the emergent evidence for a preferred spacing mode. This manifests itself in the PDF of the time between successive detections (t_d). There appears to be a loose tendency for successive hairpin structures to be 'grouped' (closely spaced) in the streamwise direction. That this preferred separation is similar to the modal peak witnessed in the PDF of time between successive VITA detections would suggest that the hairpin events are born in the near-wall region, where the spacing between adjacent births is to some degree determinable (at approximately $x^+ \approx 300$).

The overall view we are left with, is that for the Reynolds number studied here ($Re_\theta \approx 1100$) the turbulent boundary layer may be considered as little more than an amalgamation of hairpin vortices. All of the principle coherent features that typify turbulent boundary layers, from near-wall shear layers and quasi-streamwise vortices, through to lifted spanwise vortices and large-scale interfacial bulging in the wake-region, can be described and explained within a simple hierarchical population of hairpin structures.

As a footnote, we have also found that the selective (passive) removal or disruption of certain of these hairpin scales can produce large and prolonged skin friction reduction. This would seem to suggest a potential for control strategies that set out to target larger-scale structures (rather than the more usual assault on near-wall quasi-streamwise structures). For the future, we would be interested in modifying the boundary layer by actively sensing and then actuating on these structures.

REFERENCES

ADRIAN, R. J. 2002 Scaling and the relationship to structure. *IUTAM Symposium on Reynolds Number Scaling in Turbulent Flow*, Princeton, NJ.

ADRIAN, R. J., MEINHART, C. D., TOMKINS, C. D. 2000 Vortex organisation in the outer region of the turbulent boundary layer. *J. Fluid Mech.* **422**, 1–54.

BOGARD, D. G. & TIEDERMAN, W. G. 1986 Burst detection with single-point velocity measurements. *J. Fluid Mech.* **162**, 389–413.

CHRISTENSEN, K. T. & ADRIAN, R. J. 2001 Statistical evidence of hairpin vortex packets in wall turbulence. *J. Fluid Mech.* **431**, 433–443.

HUTCHINS, N., CHOI, K.-S. 2002 Towards a greater understanding of turbulent skin friction reduction. *ASME FED Paper*, FEDSM2002-31060. Fluids Engineering Division Summer Meeting.

KLINE, S. J., REYNOLDS, W. C., SCHRAUB, F. A., RUNSTADLER, P. W. 1967 The structure of turbulent boundary layers. *J. Fluid. Mech.* **30**(4), 741–773.

MARUŠIĆ, I. 2001 On the role of large-scale structures in wall turbulence. *Phys. Fluids* **13**(8), 735–743.

PANTON, R. L. 2001a Overview of the self-sustaining mechanisms of wall turbulence. *AIAA paper* 2001-2911.

PANTON, R. L. 2001b Overview of the self-sustaining mechanisms of wall turbulence. *Progress in Aerospace Sciences* **37**, 341–383.

ROBINSON, S. K. 1991 Coherent motions in the turbulent boundary layer. *Annu. Rev. Fluid Mech.* **23**, 601–39.

SCHOPPA, W. & HUSSAIN, F. 2000 Coherent structure dynamics in near-wall turbulence. *Fluid Dyn. Res.* **26**, 119-139.